Exponential Orthogonality Catastrophe in Single-Particle and Many-Body Localized Systems

Dong-Ling Deng, J. H. Pixley, Xiaopeng Li, and S. Das Sarma
Condensed Matter Theory Center and Joint Quantum Institute,
Department of Physics, University of Maryland, College Park, MD 20742-4111, USA

We investigate the statistical orthogonality catastrophe (StOC) in single-particle and many-body localized systems by studying the response of the many-body ground state to a local quench. Using scaling arguments and exact numerical calculations, we establish that the StOC gives rise to a wave function overlap between the pre- and post-quench ground states that has an *exponential* decay with the system size, in sharp contrast to the well-known power law Anderson orthogonality catastrophe in metallic systems. This exponential decay arises from a statistical charge transfer process where a particle can be effectively "transported" to an arbitrary lattice site. In a many-body localized phase, this non-local transport and the associated exponential StOC phenomenon persist in the presence of interactions. We study experimental consequences of the exponential StOC on Loschmidt echo and spectral function, establishing that this phenomenon should be observable in cold atomic experiments through Ramsey interference and radio-frequency spectroscopy.

The response of many-body states to local quenches can be remarkably drastic; even an arbitrarily weak local perturbation can substantially modify the structure of the final ground state. As shown in the seminal work by Anderson [1], the overlap between the ground states of a metallic (i.e. extended states) system with ($|G'\rangle$) and without ($|G\rangle$) a local perturbation has a power-law decay in the system size $F \equiv |\langle G|G'\rangle| \sim L^{-\gamma}$, where $\gamma > 0$ is a function of the scattering phase shift created by the local quench, and thus the overlap vanishes in the thermodynamic limit (and hence an infrared 'catastrophe'). This phenomenon is the celebrated Anderson orthogonality catastrophe (AOC) [2], which has far-reaching consequences in various contexts, ranging from the x-ray edge singularity [2] and Kondo effect [3–7] to Luttinger liquids [8–12] and resonant tunneling in mesoscopic structures [13–18]. Moreover, a power-law multifractal orthogonality catastrophe (OC) can even occur at random singlet quantum critical points [19].

Quantum localized systems, both single-particle [20] and many-body localized (MBL) [21–24], show a cornucopia of intriguing properties, such as violation of ergodicity and emergent integrability [25–27]. MBL has attracted tremendous attention recently due to the breakdown of conventional quantum statistical mechanics and the existence of infinite-temperature dynamical quantum phase transitions [28] that appear to defy any description within a conventional formalism [29, 30]. Despite extensive research in the subject, the orthogonality catastrophe, a compelling phenomenon well studied in diffusive metals [2, 31, 32], remains largely unexplored for localized systems [33]. Very recently, in an important paper [34], a new idea of statistical orthogonality catastrophe (StOC) has been introduced for the one dimensional (1D) localized Anderson model.

Here, we study the StOC in single-particle and many-body localized systems (see Fig. 1). Through scaling arguments and exact diagonalization, we show that StOC gives rise to a wave function overlap that is *exponentially* suppressed in the system size and is much stronger, albeit statistical in nature, than the well-studied power-law AOC in extended systems. In particular, by studying both 1D Anderson and Aubry-Andre (AA) models (both with and without interactions) we show that the exponential StOC is a generic many-body phenomenon in localized systems (both single-particle and many-body localized) with a typical wave function overlap $F_{\text{typ}} \equiv \exp\left(\overline{\log F}\right)$ going as

$$F_{\text{typ}} \sim \exp\left(-\beta L\right), \qquad (1)$$

as shown in Fig. 2. Here, $\beta > 0$ is related to the localization length and the strength of the local quench. Moreover, by using the kernel polynomial method [35], we calculate the spectral function and Loschmidt echo, which allows us to demonstrate that they manifest certain unique features that are related to exponential StOC and can be directly observed in a cold atom experiment through Ramsey interference or radio-frequency spectroscopy [36]. Since the fundamental nature of Anderson and AA localizations are qualitatively different, with quantum interference and quantum gap spectrum playing the key role respectively, we hypothesize that all localized systems (single-particle or many-body) are characterized by the exponential StOC established in the current work.

Model system.— In this work, we consider a class of 1D interacting fermionic initial Hamiltonians defined as

$$H_I = \sum_{j=-L/2+1}^{L/2} -J(a_j^\dagger a_{j+1} + h.c.) + \mu_j n_j + U n_j n_{j+1}, \quad (2)$$

where a_j $(a_j^\dagger)$ are fermionic annihilation (creation) operators, $n_j = a_j^\dagger a_j$ is the corresponding fermion number operator, J is the nearest-neighbour hopping strength, and $U > 0$ is the nearest-neighbor interaction. Depending on how we choose the local chemical potential, the model in
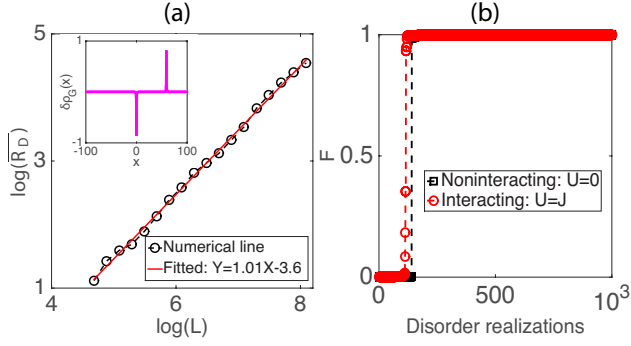
FIG. 1: Nonlocal charge transfer and StOC for the AA model. (a) Scaling of the radius of zone of disturbance ($\overline{R_D}$) with system size in the non-interacting AA model. A linear scaling $\overline{R_D} \sim 0.03L$ is obtained. To suppress statistical errors, we averaged over 10^4 different values of ϕ (evenly distributed in $[-\pi, \pi]$). Inset: nonlocal adiabatic charge transfer for a fixed $\phi = 5\pi/4$. A particle on site 0 is transferred to a distant location (near site 60) by the time-dependent local potential V_0. (b) Many-body ground state overlaps sorted over 10^3 different values of ϕ for the AA model with and without interaction. Depending on whether there is a charge transfer or not during the adiabatic process, the overlap F is vanishing or close to unity, leading to a 'statistical' version of OC with probability P around 0.25. Here we fix $v_0 = 0.4\lambda = 1.6J$.

Eq. (2) can be reduced to either the Anderson model [20] if the local potential μ_i is drawn from a uniform random distribution between $[-W, W]$, or the AA model [37, 38] if $\mu_j = \lambda \cos(2\pi\alpha j + \phi)$, where λ is the strength of the potential, with α an irrational number and ϕ a random phase. Both Anderson and AA models have been extensively studied in the context of many-body localization (see Ref. [28, 39, 40]). To unify the notation between the two models we will use g to denote W and λ respectively for the 1D Anderson and AA model. In both cases, we start with a localized many-body ground state $|G\rangle$, we then quench the model by introducing a local impurity into the Hamiltonian through an onsite potential $V_0 = v_0 a_0^\dagger a_0$ ($v_0 > 0$) at site 0 and arrive at a final Hamiltonian $H_F = H_I + V_0$, with a new ground state $|G'\rangle$. We investigate the asymptotic behavior of the many-body ground state overlap (fidelity) defined by $F \equiv |\langle G|G'\rangle|$, as a function of the system size.

Charge transfer— We consider a time-dependent Hamiltonian $H(t) = H_I + V_0(t/\tau)$, where H_I is a static Hamiltonian describing a localized system and $V_0(t/\tau)$ a time-dependent local potential at site 0, and τ is chosen large enough so that adiabaticity is maintained. The time dependence of the local potential is $V_0(-\infty) = 0$ and $V_0(\infty) = v_0 a_0^\dagger a_0$. In order to characterize the charge response, we define the change of density as $\delta\rho(x) \equiv \langle n_x \rangle_{t=\infty} - \langle n_x \rangle_{t=-\infty}$, where $\langle n_x \rangle_t = \langle G(t)|n_x|G(t)\rangle$, $|G(t = -\infty)\rangle = |G\rangle$ and $|G(t = \infty)\rangle = |G'\rangle$ denote respectively the instantaneous initial and final ground states of $H(t)$ [34]. As a result of the local potential, for

certain disorder realizations such that $\mu_0 < 0$, $\mu_0 + v_0 > 0$ charge will be transferred from site 0 to an arbitrary site R_F (see the inset of Fig. 1 (a)), with $1 < |R_F| \leq L/2$ (see our coordinate choice in Eq. (2)), and therefore the initial and final ground state wave functions will be orthogonal ($F \to 0$ in the thermodynamic limit). Whereas for other realizations no charge transfer will take place and therefore $F \approx 1$. It is in this sense that the StOC in localized systems is *statistical*, depending on specific random potential realizations. This is captured in our numerical calculations for the AA model with and without interactions as shown in Fig. 1(b), where we plot F sorted in magnitude over 10^3 different random realizations of ϕ. For $U = 0$, we find an OC with probability $P(-v_0 < \mu_0 < 0) \approx 0.25$, whereas for $U/J = 1$ the probability is reduced slightly. We also establish StOC for the interacting Anderson model [41].

In order to quantify the distance the charge will move, we consider the so-called radius of the "zone of disturbance" over which charge transfer takes place

$$R_D \equiv \frac{\int_{-L/2}^{L/2} |x\delta\rho(x)|dx}{\int_{-L/2}^{L/2} |\delta\rho(x)|dx}. \tag{3}$$

As a result of the charge transfer landing on any arbitrary site the disorder average of R_D can have a very wide spatial distribution, giving rise to the scaling $\overline{R_D} \sim \eta(g, U)L$, as shown in Fig. 1 (a) for the non-interacting AA model, in agreement with Ref. [34] for the 1D non-interacting Anderson model. In addition, we also establish $\overline{R_D} \sim L$ in the MBL phase of both interacting 1D Anderson and AA models [41]. Thus, we have established $\overline{R_D} \sim L$ for the ground state of generic localized systems, irrespective of single-particle or many-body localized.

Finite size scaling of F— Here, we establish the leading finite size scaling of F in the non-interacting limit based on the dynamic charge transfer picture presented above. We then generalize the scenario to the MBL case. We begin by considering N particles in the localized phase. The many-body ground state is constructed by filling the N lowest single-particle eigenstates, which have localized wave functions going as $\phi_n(x) \propto \exp(-|x-x_n|/\xi)$, with x_n the localization center and ξ the single-particle localization length. Focusing on a disorder realization that transfers charge from site 0 to site R_f, the leading contribution to the overlap goes as

$$F \sim \int dx \phi_0(x)\phi'_f(x) \sim e^{-|R_f|/\xi}, \tag{4}$$

with $\phi'_f(x)$ referring to the post-quench single-particle wave function. Consequently, the disorder averaged $\overline{\log F} \sim -\overline{|R_f|}/\xi$, where $\overline{|R_f|}$ is the averaged distance of charge transfer, which has the same scaling as $\overline{R_D}$, i.e., $\overline{|R_f|} \sim \overline{R_D} \sim L$. Thus, we arrive at one of our main results $\overline{\log F} \sim -\beta L$, and
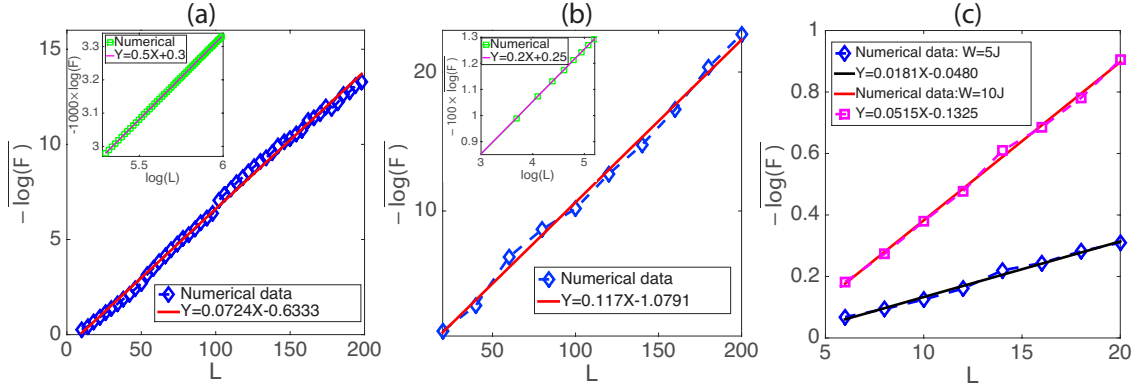
$$F_{\text{typ}} \sim \exp(-\beta L), \quad \beta = P/4\xi, \tag{5}$$

FIG. 2: Exponential StOC in single-particle and many-body localized systems. (a) Anderson model with $v_0 = 0.4W = 4J$ and $U = 0$. $\overline{\log(F)}$ is obtained by averaging over 10^5 disorder realizations. The typical fidelity has an exponential decay $F_{\text{typ}} \sim e^{-0.0724L}$. Inset: AOC for a clean (metallic) system with $W = 0$, $v_0 = 0.2J$ and $U = 0$. The overlap has a power-law decay $F \sim L^{-5 \times 10^{-4}}$, as expected from Anderson [1]. (b) AA model with $v_0 = 0.4\lambda = 1.6J$ and $U = 0$. $\overline{\log(F)}$ is obtained by averaging over 10^5 different values of ϕ, which are uniformly distributed in $[-\pi, \pi]$. The typical fidelity has an exponential decay $F_{\text{typ}} \sim e^{-0.117L}$. Inset: OC with power-decaying overlap $F_{\text{typ}} \sim L^{2 \times 10^{-3}}$ in the delocalized region with $\lambda = 0.25v_0 = 0.1J$. (c) Anderson model a MBL phase with $U = J$ and $v_0 = 0.4W$. $\overline{\log(F)}$ is obtained by averaging over 10^4 disorder realizations. The typical fidelity has a exponential decay $F_{\text{typ}} \sim e^{-0.0515L}$ ($F_{\text{typ}} \sim e^{-0.0181L}$) for $W = 10J$ ($W = 5J$).

where P is the probability of creating the charge transfer event, i.e. $P = v_0/(2W)$ and $P(-v_0 < \mu_0 < 0)$ for the non-interacting Anderson and AA models, respectively.

The above argument can also carry over to the MBL case via the 'l-bits' formalism where the 'l-bits' are related to charge degrees of freedom by quasi-local unitary transformations and their interactions are exponentially local [26, 27]. We then expect from the charge transfer picture that the overlap between interacting many-body ground states before and after the charge transfer to go as $F \sim \exp(-|R_f|/\xi_{\text{MBL}})$, where ξ_{MBL} is the many-body localization length that can be computed through local integrals of motion [42]. Consequently for this many-body case, F_{typ} still approaches zero exponentially as the non-interacting case, yet with $\beta = P_{U \neq 0}/\xi_{\text{MBL}}$. We now turn to exact numerical calculations to put the scaling analysis on a solid footing.

Numerical results.—We now present our numerical results in order to establish the exponential StOC for localized systems. We use exact diagonalization to diagonalize H_I and H_F to obtain the energy spectrum and eigenstates. For the noninteracting case, the many-body ground states are constructed by simply filling the single-particle eigenstates and the overlaps are calculated via determinants (see Supplemental Material [41]). For the interacting case, the overlaps can be computed directly by inner products of $|G\rangle$ and $|G'\rangle$ after an exact diagonalization of the many-body hamiltonian. We then calculate the wave function overlap (F) averaged over different disorder realizations for both Anderson and AA models.

Our numerical results for the StOC in the Anderson and AA models are shown in Fig. 2, which clearly confirms our scaling analysis, and establishes the exponen-
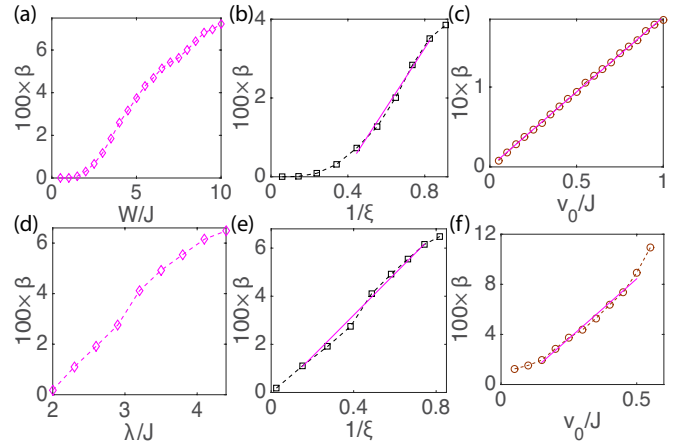

FIG. 3: β dependences for the Anderson ((a), (b), and (c)) and AA ((d), (e), and (f)) models in the noninteracting limit. The other parameters are chosen as $v_0 = 0.4W$ ($v_0 = 0.4\lambda$) in (a) and (b) ((d) and (e)); $W = 10J$ in (c) and $\lambda = 4J$ in (f). Dashed magenta lines are fits to the linear relationships in each case.

tial StOC $F_{\text{typ}} \sim \exp(-\beta L)$. For the sake of comparison, we have also plotted the results for the clean (metallic, $W = 0$) limit of the Anderson model and for the delocalized phase of the AA model ($\lambda/J < 2$), respectively. For these extended states, the overlaps follow a power-law decay, as expected from AOC [1]. For the non-interacting case we are able to reach sufficiently large system sizes, whereas in the MBL phase we are limited to $L = 24$ as our largest system.

In Fig. 3, we show the dependence of β on W, λ, ξ and v_0 in the non-interacting limit. First, we focus on

the strength of the on site potential, which is related to the localization length as $1/\xi \sim |g - g_c|^\nu$ near g_c with a localization length exponent ν (for the 1D Anderson and AA models, g_c is 0 and 2λ, respectively). Deep in the localized phase ξ saturates to the lattice spacing, whereas it diverges on approaching the localization transition point. We thus expect β to be zero at $g = g_c$ and to increase as we increase g from g_c, which is in excellent agreement with our numerical calculations. In addition, the scaling analysis also predicts $\beta \propto 1/\xi$. We compute the localization length directly from the decay of the single-particle wavefunction $\phi(x)$ from its maximal value (in absolute value) and then average over disorder realizations. Close to the localization transition and deep within the localized phase such a method of calculating ξ suffers from large numerical error, nonetheless in the intermediate parameter regime we establish a clear linear relation. Finally, we come to the dependence of β on v_0 for a fixed g. The results are in good agreement with $\beta \propto v_0$, which allows us to conclude that our numerical results are consistent with $\beta = P/4\xi$, and thus provide another independent confirmation of our scaling analysis.

Experimental detection. —The AOC has far-reaching consequences for several dynamical phenomena, such as X-ray edge singularity in metals [2] and power-law suppressed Loschmidt echo for ultracold atoms in the long time limit [43]. We expect the exponential StOC in localized systems to have significant implications in similar experimental settings. In a setup proposed to probe the OC physics [43–45], a nature experimentally measurable quantity to characterize the exponential StOC is the typical Loschmidt echo defined as $S_{\mathrm{typ}}(t) \equiv \exp(\overline{\log |S(t)|})$, where

$$S(t) = \langle G|e^{iH_I t}e^{-iH_F t}|G\rangle. \tag{6}$$

In Fig. 4 (a) we show $S_{\mathrm{typ}}(t)$ for the Anderson model [46]. As a result of the StOC and the localized nature of the many body ground state we find $S_{\mathrm{typ}}(t)$ saturates to a nonzero value in the long-time limit. This is in sharp contrast to the metallic case where $|S(t)|$ has a power-law decay due to the AOC [43]. Another quantity that is also directly measurable in experiments is the spectral function (which is related to the "hole" Green function in the AOC literature [2]) $A(\omega) = \sum_{n'} |\langle G|n'\rangle|^2 \delta(\omega - (E_{n'} - E_G))$, where $|n'\rangle$ is the n'-th eigenstate of H_F with eigen energy $E_{n'}$ and E_G is the ground state energy of H_I. Using the kernel polynomial method [35], we calculate the disorder-averaged spectral function for both the AA and Anderson models (see [41]). As shown in Fig. 4(b) and (c), the spectral function exhibits two peaks with exponentially decaying tails, which are unique features of the exponential StOC in localized systems (whereas in the AOC, $A(\omega)$ has only one peak and a power-law dependence [2]).

With the recent experimental realizations of single-particle [47–49] and many-body localization [50–52], the
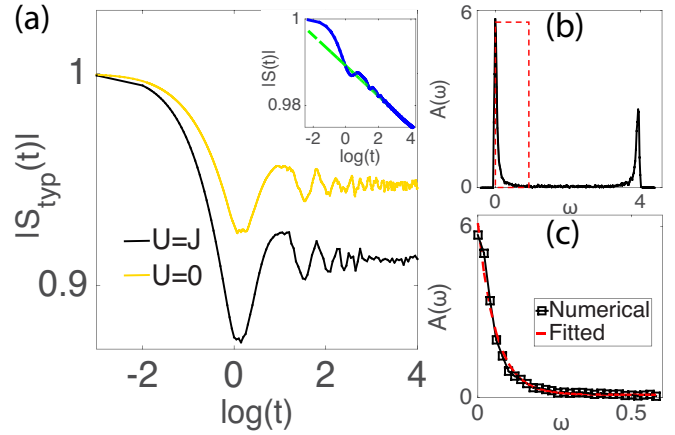

FIG. 4: Numerical simulations of the typical Loschmidt echo and spectral functions. (a) The typical Loschmidt echo as a function of time for the Anderson model with and without interaction. Inset: Loschmidt echo in the clean limit, which has a power-law decay at long time. (b) The disorder-averaged spectral function for the interacting Anderson model. Unlike the metallic or the ordinary band-insulator cases, $A(\omega)$ for localized systems has two divergent peaks at either $\omega = 0$ or $\omega = v_0$ and non-zero weight between $(0, v_0)$. (c) Zooming in on the red rectangular region of (b). Near $\omega = 0$, an exponential decay $A(\omega) \sim 6 \times e^{-17.1\omega} + 0.1$ is obtained. The parameters are chosen the same as in Fig.2 (see [41] for more details).

above intriguing features could be experimentally observed with present techniques. Considering a ultracold atom experiment for instance, the localized ground states could be achieved by adiabatic ramping and the local quench can be switched on and off by manipulating locally two-level atoms (the impurity atoms of a strongly imbalanced mixtures [53, 54]), and the Loschmidt echo and the spectral function can be directly measured through Ramsey interference and radio-frequency spectroscopy, respectively (see Ref. [43–45] for details). In electronic materials, nontrivial effects of the exponential StOC may have already been observed in recent experiments of quantum electron glasses [55, 56], where dramatic sluggish dynamics have been reported.

To conclude, we have established a statistical exponential orthogonality catastrophe in both single-particle and many-body localized systems. We introduced scaling arguments to explain this 'stronger' catastrophe. Using exact numerical calculations we have verified the scaling analysis and its generalization to the MBL case. The exponential StOC can be used as a diagnostic tool to identify localization and could be directly observed in cold-atomic or other mesoscopic systems with current technologies.

percomputing resources (http://www.it.umd.edu/hpcc) made available in conducting the research reported in this paper.

———————

[1] P. W. Anderson, Phys. Rev. Lett. **18**, 1049 (1967).
[2] G. D. Mahan, *Many-particle physics* (Springer, 2000).
[3] M. Hentschel and F. Guinea, Phys. Rev. B **76**, 115407 (2007).
[4] G. Yuval and P. W. Anderson, Phys. Rev. B **1**, 1522 (1970).
[5] H. E. Türeci, M. Hanl, M. Claassen, A. Weichselbaum, T. Hecht, B. Braunecker, A. Govorov, L. Glazman, A. Imamoglu, and J. von Delft, Phys. Rev. Lett. **106**, 107402 (2011).
[6] C. Latta, F. Haupt, M. Hanl, A. Weichselbaum, M. Claassen, W. Wuester, P. Fallahi, S. Faelt, L. Glazman, J. von Delft, *et al.*, Nature **474**, 627 (2011).
[7] W. Münder, A. Weichselbaum, M. Goldstein, Y. Gefen, and J. von Delft, Phys. Rev. B **85**, 235104 (2012).
[8] V. Meden, P. Schmitteckert, and N. Shannon, Phys. Rev. B **57**, 8878 (1998).
[9] A. O. Gogolin, Phys. Rev. Lett. **71**, 2995 (1993).
[10] M. Pustilnik, M. Khodas, A. Kamenev, and L. I. Glazman, Phys. Rev. Lett. **96**, 196405 (2006).
[11] A. Imambekov, T. L. Schmidt, and L. I. Glazman, Rev. Mod. Phys. **84**, 1253 (2012).
[12] A. Imambekov and L. I. Glazman, Science **323**, 228 (2009).
[13] K. A. Matveev and A. I. Larkin, Phys. Rev. B **46**, 15337 (1992).
[14] D. A. Abanin and L. S. Levitov, Phys. Rev. Lett. **94**, 186803 (2005).
[15] N. d'Ambrumenil and B. Muzykantskii, Phys. Rev. B **71**, 045326 (2005).
[16] M. Hentschel, D. Ullmo, and H. U. Baranger, Phys. Rev. B **72**, 035310 (2005).
[17] A. K. Geim, P. C. Main, N. La Scala, L. Eaves, T. J. Foster, P. H. Beton, J. W. Sakai, F. W. Sheard, M. Henini, G. Hill, and M. A. Pate, Phys. Rev. Lett. **72**, 2061 (1994).
[18] D. A. Abanin and L. S. Levitov, Phys. Rev. Lett. **93**, 126802 (2004).
[19] R. Vasseur and J. E. Moore, Phys. Rev. B **92**, 054203 (2015).
[20] P. W. Anderson, Phys. Rev. **109**, 1492 (1958).
[21] D. Basko, I. Aleiner, and B. Altshuler, Annals of physics **321**, 1126 (2006).
[22] I. V. Gornyi, A. D. Mirlin, and D. G. Polyakov, Phys. Rev. Lett. **95**, 206603 (2005).
[23] E. Altman and R. Vosk, Annu. Rev. Condens. Matter Phys. **6**, 383 (2015).
[24] R. Nandkishore and D. A. Huse, Annu. Rev. Condens. Matter Phys. **6**, 15 (2015).
[25] V. Rosa, M. Müllerc, and A. Scardicchiob, Nucl. Phys. B **891**, 420 (2015).
[26] D. A. Huse, R. Nandkishore, and V. Oganesyan, Phys. Rev. B **90**, 174202 (2014).
[27] M. Serbyn, Z. Papic, and D. A. Abanin, Phys. Rev. Lett. **111**, 127201 (2013).
[28] A. Pal and D. A. Huse, Phys. Rev. B **82**, 174411 (2010).
[29] A. C. Potter, R. Vasseur, and S. A. Parameswaran, Phys. Rev. X **5**, 031033 (2015).
[30] R. Vosk, D. A. Huse, and E. Altman, Phys. Rev. X **5**, 031032 (2015).
[31] Y. Chen and J. Kroha, Phys. Rev. B **46**, 1332 (1992).
[32] I. L. Aleiner and K. A. Matveev, Phys. Rev. Lett. **80**, 814 (1998).
[33] Y. Gefen, R. Berkovits, I. V. Lerner, and B. L. Altshuler, Phys. Rev. B **65**, 081106 (2002).
[34] V. Khemani, R. Nandkishore, and S. L. Sondhi, Nat. Phys. **11**, 560 (2015).
[35] A. Weiße, G. Wellein, A. Alvermann, and H. Fehske, Rev. Mod. Phys. **78**, 275 (2006).
[36] M. Knap, A. Shashi, Y. Nishida, A. Imambekov, D. A. Abanin, and E. Demler, Phys. Rev. X **2**, 041020 (2012).
[37] S. Aubry and G. André, Ann. Israel Phys. Soc. **3**, 18 (1980).
[38] S. Iyer, V. Oganesyan, G. Refael, and D. A. Huse, Phys. Rev. B **87**, 134202 (2013).
[39] E. Abrahams, P. W. Anderson, D. C. Licciardello, and T. V. Ramakrishnan, Phys. Rev. Lett. **42**, 673 (1979).
[40] S. Bera, H. Schomerus, F. Heidrich-Meisner, and J. H. Bardarson, Phys. Rev. Lett. **115**, 046603 (2015).
[41] See Supplemental Material at [URL will be inserted by publisher] for more details on: the calculation of the overlap for free fermionic systems, StOC and charge transfer for interacting Anderson and AA models, Loschmidt echo, and spectral function..
[42] A. Chandran, I. H. Kim, G. Vidal, and D. A. Abanin, Phys. Rev. B **91**, 085425 (2015).
[43] M. Knap, A. Shashi, Y. Nishida, A. Imambekov, D. A. Abanin, and E. Demler, Phys. Rev. X **2**, 041020 (2012).
[44] J. Goold, T. Fogarty, N. Lo Gullo, M. Paternostro, and T. Busch, Phys. Rev. A **84**, 063632 (2011).
[45] A. Sindona, J. Goold, N. Lo Gullo, S. Lorenzo, and F. Plastina, Phys. Rev. Lett. **111**, 165303 (2013).
[46] In contrast to the wave function overlap, we find that $S(t)$ is a self averaging quantity and our conclusions are also applicable to $\overline{|S(t)|}$.
[47] J. Billy, V. Josse, Z. Zuo, A. Bernard, B. Hambrecht, P. Lugan, D. Clément, L. Sanchez-Palencia, P. Bouyer, and A. Aspect, Nature **453**, 891 (2008).
[48] S. Kondov, W. McGehee, J. Zirbel, and B. DeMarco, Science **334**, 66 (2011).
[49] G. Roati, C. D'Errico, L. Fallani, M. Fattori, C. Fort, M. Zaccanti, G. Modugno, M. Modugno, and M. Inguscio, Nature **453**, 895 (2008).
[50] S. S. Kondov, W. R. McGehee, W. Xu, and B. DeMarco, Phys. Rev. Lett. **114**, 083002 (2015).
[51] M. Schreiber, S. S. Hodgman, P. Bordia, H. P. Lüschen, M. H. Fischer, R. Vosk, E. Altman, U. Schneider, and I. Bloch, Science **349**, 842 (2015).
[52] J. Smith, A. Lee, P. Richerme, B. Neyenhuis, P. W. Hess, P. Hauke, M. Heyl, D. A. Huse, and C. Monroe, arXiv preprint arXiv:1508.07026 (2015).
[53] M. W. Zwierlein, A. Schirotzek, C. H. Schunck, and W. Ketterle, Science **311**, 492 (2006).
[54] Y.-a. Liao, A. S. C. Rittner, T. Paprotta, W. Li, G. B. Partridge, R. G. Hulet, S. K. Baur, and E. J. Mueller, Nature **467**, 567 (2010).
[55] Z. Ovadyahu, Phys. Rev. Lett. **115**, 046601 (2015).
[56] Z. Ovadyahu, Phys. Rev. Lett. **99**, 226603 (2007).

I. SUPPLEMENTAL MATERIAL FOR "EXPONENTIAL ORTHOGONALITY CATASTROPHE IN SINGLE-PARTICLE AND MANY-BODY LOCALIZED SYSTEMS"

A. Calculations of ground-state overlaps for free fermions

In this section, we provide the details on how we calculate the ground-state overlap for free fermions. As in the main text, we denote by $|G\rangle$ and $|G'\rangle$ the ground states of H_I and H_F. Since we only consider the free fermion case, H_I (H_F) can be written as $H_I = \sum_{ij} a_i^\dagger (\mathcal{H}_I)_{ij} a_j$ ($H_F = \sum_{ij} a_i^\dagger (\mathcal{H}_F)_{ij} a_j$), where $\mathcal{H}_I$ ($\mathcal{H}_F$) is the so called kernel Hamiltonian. One can diagonalize $\mathcal{H}_I$ ($\mathcal{H}_F$) by a unitary transformation $\mathcal{U}$ ($\mathcal{V}$): $\mathcal{H}_I = \mathcal{U}^\dagger \mathcal{E}_I \mathcal{U}$ ($\mathcal{H}_F = \mathcal{V}^\dagger \mathcal{E}_F \mathcal{V}$) to find the single-particle eigenmodes $b_j = \sum_k \mathcal{U}_{jk} a_k$ ($c_j = \sum_k \mathcal{V}_{jk} a_k$). Here $\mathcal{E}_I = \text{diag}(\epsilon_1^I, \epsilon_2^I, \cdots)$ ($\mathcal{E}_F = \text{diag}(\epsilon_1^F, \epsilon_2^F, \cdots)$) is a diagonal matrix. Suppose the lattice size is L and the total particle number is N. For free fermionic systems, the ground states of H_I and H_F are constructed by filling the lowest N single-particle eigenstates:

$$|G\rangle = \prod_j^N b_j^\dagger |0\rangle,$$

$$|G'\rangle = \prod_j^N c_j^\dagger |0\rangle.$$

Thus the overlap reads:

$$F \equiv |\langle G|G'\rangle| = |\langle 0| \prod_j^N b_j \prod_k^N c_k^\dagger |0\rangle|. \tag{7}$$

Computing F directly from Eq. (7) is challenging. However, we can simplify Eq. (7) by expressing the eigenmodes $c_l^\dagger$s as a combination of $b_l^\dagger$s $c_k^\dagger = \sum_m (\mathcal{V}^\dagger)_{km} a_m^\dagger = \sum_m (\mathcal{V}^\dagger)_{km} (\sum_n \mathcal{U}_{mn} b_n^\dagger) = \sum_{mn} (\mathcal{V}^\dagger)_{km} \mathcal{U}_{mn} b_n^\dagger$, which corresponds to a change of basis. Defining another matrix $A = \mathcal{V}^\dagger \mathcal{U}$, we have $c_k^\dagger = \sum_n A_{kn} b_n^\dagger$ and consequently

$$F = |\langle 0| \prod_j^N b_j \prod_k^N \sum_n A_{kn} b_n^\dagger |0\rangle|.$$

Noting that $\{b_j, b_n^\dagger\} = \delta_{jn}$, $b_n|0\rangle = 0$ and $(b_n^\dagger)^p = 0$ for all n and $p > 1$, we arrive at a greatly simplified formula

$$F = |\det B|, \tag{8}$$

where $B_{ij} = A_{ij}$ ($1 \le i,j \le N$) is a matrix with elements taken from A. The above equation is very useful in our numerical calculations. With this formula, we are able to calculate the overlap efficiently for different random realizations.

B. More results on charge transfer and orthogonality catastrophe

In the main text, we have established an exponential statistical orthogonality catastrophe in localized systems and its relation to adiabatic charge transfer. Here we show additional numerical results to support our claim.

1. The Anderson model

In Fig. 5, we plot the scaling of $\overline{R_D}$ with system size and the StOC for the Anderson model. From Fig. 5(a), one indeed obtain a linear scaling $\overline{R_D} \sim L$ for the interacting Anderson model in the MBL phase, thus validating the heuristic arguments in Ref. [34]. From Fig. 5(b), we have statistical orthogonality catastrophe due to the nonlocal charge transfer, as expected. The probability of StOC for the noninteracting Anderson model is about $P \approx v_0/(2W) = 0.2$, whereas this probability is reduced for the interacting case, similar to case of the AA model (see Fig. 1 in the main text).
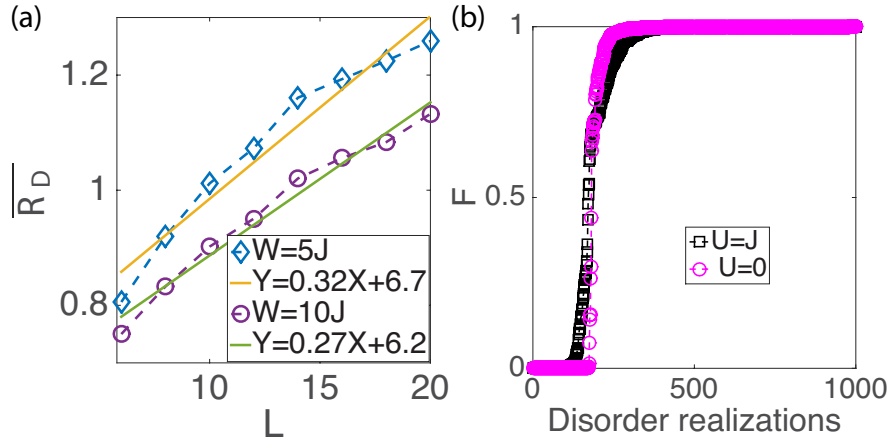
FIG. 5: Scaling of $\overline{R_D}$ and many-body ground state overlaps for the Anderson model. (a) Scaling of $\overline{R_D}$ with system size for the interacting Anderson model. Linear scalings $\overline{R_D} \sim 0.32L$ and $\overline{R_D} \sim 0.27L$ are obtained for $W = 5J$ and $W = 10J$, respectively. Here we have fixed $U = J$ and used 10^4 random realizations to suppress statistical errors. (b) Many-body ground state overlaps sorted over 10^3 disorder realizations for the Anderson model. For the interacting (noninteracting) case, the lattice size is $L = 24$ ($L = 200$). Other parameters are chosen as $v_0 = 0.4W = 4J$.
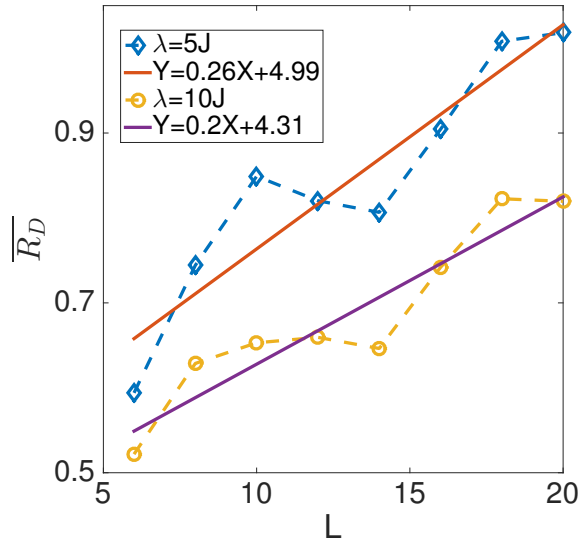

FIG. 6: Nonlocal charge transfer in the interacting Aubry-Andre model with $U = J$. $\overline{R_D}$ is obtained by averaging over 10^4 different values of ϕ evenly distributed in $[-\pi, \pi]$ and v_0 is chosen as $v_0 = 0.4\lambda$.

2. The Aubry-Andre model

In the main text, we have shown the StOC in this model for both interacting and noninteracting cases (see Fig. 1(c)). Here we show more numerical results on the charge transfer and StOC for the interacting Aubry-Andre model. In Fig. 6, we plot the scaling of the radius of zone of disturbance $\overline{R_D}$ (R_D is defined by Eq. (4) in the main text) with the system size. One may notice that the numerical lines are not exactly straight lines and there are large deviations due to the finite-size effect. Yet, it is clear that the qualitative trend is still correct. In Fig. 7, we plot the scaling of $-\overline{\log(F)}$ with the system size for the interacting AA model. Here the finite-size effect is also non-negligible. In order to clarify the role of finite size effects we compare the many body interacting case with the non-interacting results that can reach much larger systems sizes as shown in Fig. 8(a). From this figure, it is clear that the influence of interaction on $-\overline{\log(F)}$ is weak deep in the localized region. Despite the step like features at small L, as shown in Fig. 8(b) and (c) this is truly just an artifact of small system sizes, where increasing L gives rise to a clear $-\overline{\log(F)} \sim L$
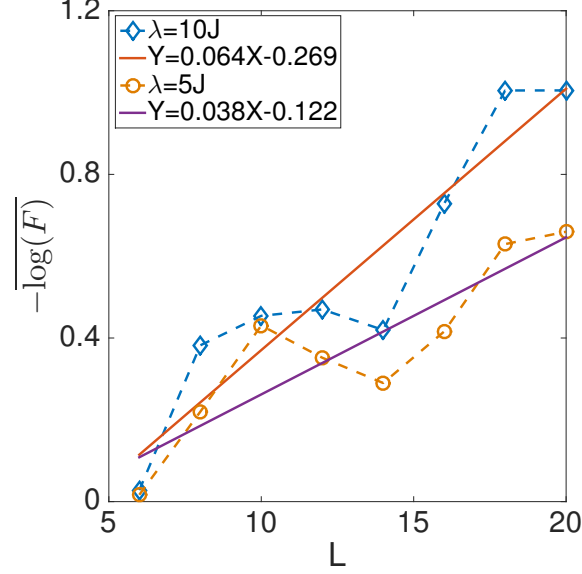
FIG. 7: Exponential statistical OC in the interacting Aubry-Andre model. Due to finite size effect, the numerical data has a large deviation from the corresponding fitted line. $-\overline{\log(F)}$ is obtained by averaging over 10^4 different values of ϕ evenly distributed in $[-\pi, \pi]$. Other parameters are chosen as $U = J$ and $v_0 = 0.4\lambda$.
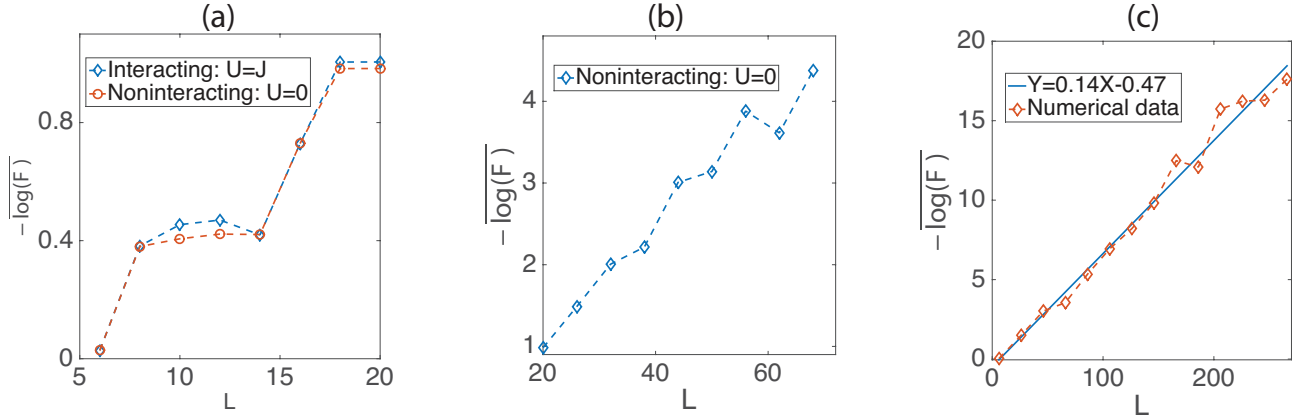

FIG. 8: (a) Comparison of exponential statistical OC in the interacting and noninteracting Aubry-Andre model. In the deep localized region ($\lambda = 10J$), the interaction does not modify $-\overline{\log(F)}$ very much. (b) and (c) plot the scaling of $-\overline{\log(F)}$ with system size for the noninteracting case. Results are obtained by averaging over 10^4 different values of ϕ evenly distributed in $[-\pi, \pi]$ and here $v_0 = 0.4\lambda = 4J$.

system size dependence. Thus, as shown in these two figures, the linearity of $-\overline{\log(F)}$ with L becomes more and more evident as the system size becomes larger and larger. As we have shown, deep in the localized phase, the presence of interactions does not quantitatively change $-\overline{\log(F)}$ by a large amount, we thus conclude that $-\overline{\log(F)}$ also goes linearly with L, giving the exponential scaling $F_{\text{typ}} \sim e^{-\beta L}$ as expected.

C. Calculations of the Loschmidt echo and spectral function

1. Calculations of the Loschmidt echo

In the main text, we have calculated the Loschmidt echo defined as:

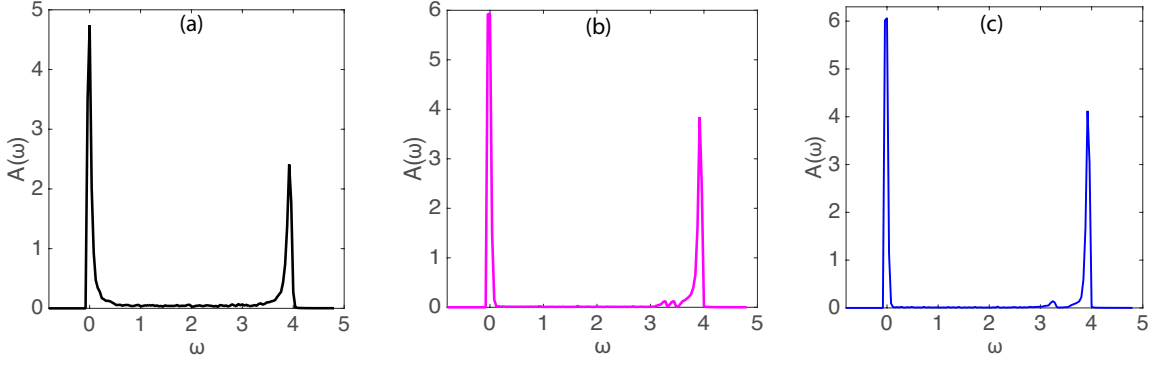$$S(t) = \langle G| e^{iH_I t} e^{-iH_F t} |G\rangle. \tag{9}$$

FIG. 9: Disorder-averaged spectral functions. (a) The Anderson model without interaction. The parameters are chosen as $W = 10J$ and $v_0 = 4J$, and the spectral function is averaged over 10^4 random realizations. (b) The AA model without interaction. (c) The AA model with interaction ($U = J$). Other parameters are chosen as $\lambda = 10J$ and $v_0 = 4J$, and $A(\omega)$ is averaged over 10^4 different values of ϕ evenly distributed in $[-\pi, \pi]$. For all these three plots, the system size $L = 20$.

A direct calculation of $S(t)$ using Eq. 9 confronts lots of computational complexity. For the noninteracting cases, the calculation can be greatly simplified. Note that $|G\rangle = \prod_j^N b_j^\dagger |0\rangle$ is the ground state of H_I, then we have $S(t) = e^{iE_G t}\langle G|e^{-iH_F t}|G\rangle$. To calculate $\langle G|e^{-iH_F t}|G\rangle$, one can do a time-evolution of each eigenmode of $\mathcal{H}_\mathcal{I}$

$$b_j(t) = e^{-iH_F t}b_j e^{iH_F t} = \sum_m \sum_k \left(e^{-i\mathcal{H}_F t}\right)_{mk} \mathcal{U}_{jk} a_k. \tag{10}$$

After $b_j(t)$ is obtained, we one can re-express $b_j(t)$ as a combination of b_l's and then the calculation of $S(t)$ is reduced to the computation of a determinant at each time t, following the same procedures in Sec. I. In Fig. 4(a) of the main text, we have shown the typical Loschmidt echo S_{typ} for the noninteracting Anderson model (the yellow curve). In this case, our lattice size is $L = 200$ and we used 10^4 random realizations. For the interacting case, calculations of $S(t)$ requires full diagonalizations of many-body Hamiltonians and our system size are limited to $L = 14$. The numerical results of $S(t)$ for the interacting Anderson model are also shown in Fig. 4(a) (the black curve) in the main text. For both interacting and noninteracting cases, $S(t)$ has various distinctive features that are related to the exponential StOC and are different from that of the Anderson OC for a metallic phase. We have also calculated the Loschmidt echo of the AA model for both interacting and noninteracting cases, and very similar features are obtained.

2. Calculations of the spectral function

In the main text, we have defined the dynamic spectral function as

$$A(\omega) = \sum_{n'} |\langle G|n'\rangle|^2 \delta(\omega - (E_{n'} - E_G)). \tag{11}$$

A direct calculation of $A(\omega)$ using Eq. 11 would also require a full diagonalizations of the many-body Hamiltonians to obtain the eigenstates $|n'\rangle$. We can avoid this by using the so called kernel polynomial method (KPM) [35] to calculate $A(\omega)$ for system size up to $L = 24$. For each random realization of H_I, we use the Lanczos algorithm to find the ground state $|G\rangle$ and the corresponding eigen-energy E_G. We then define a new Hamiltonian $H' = H_F - E_G$ to shift the eigen energies of H_F and follow the standard procedures of KPM (see Ref. [35] for details). In order to fit the spectrum into the interval $[-1, 1]$ (within which the Chebyshev polynomials are defined) we apply a simple linear transformation to H':

$$\tilde{H}' = (H' - b)/a, \tag{12}$$

where $a = (E'_{\max} - E'_{\min})/(2 - \epsilon)$ and $b = (E'_{\max} + E'_{\min})/2$; Here ϵ is a small cutoff parameter introduced to avoid stability problems ($\epsilon = 10^{-3}$ is chosen in our numerical calculations); $E'_{\max}$ and $E'_{\min}$ are the maximal and minimal eigen energies of H', respectively. Both $E'_{\max}$ and $E'_{\min}$ can be obtained by directly diagonalizing H' using Lanczos algorithm. Then the spectral function can be expanded in Chebyshev polynomials [35]

$$A(\tilde{\omega}) = \frac{1}{\pi\sqrt{1 - \tilde{\omega}^2}} \left(g_0\nu_0 + 2\sum_{k=1}^{K-1} g_k\nu_k T_k(\tilde{\omega})\right), \tag{13}$$

where $T_k(x) = \cos[k \arccos(x)]$ are the Chebyshev polynomials and $g_k = [(K-k+1)\cos\frac{k\pi}{K+1} + \sin\frac{k\pi}{K+1}\cot\frac{\pi}{K+1}]/(K+1)$ are the coefficients of the Jackson kernel; the moments $\nu_k = \langle G|T_k(-\tilde{H}')|G\rangle$ can be obtained iteratively based on the recursion relations of the Chebyshev polynomials

$$T_0(x) = 1, \ T_{-1}(x) = T_1(x) = x, \ \text{and} \ T_{k+1}(x) = 2xT_k(x) - T_{k-1}(x). \tag{14}$$

After $A(\tilde{\omega})$ is obtained, one can do a rescaling $\tilde{\omega} \to \omega = a\tilde{\omega} + b$ to obtain $A(\omega)$. In Fig. 4 (b) in the main text, we have plotted the disorder-averaged spectral function for the interacting Anderson model. In this plot, we have $L = 20$ and used 10^4 random realizations. The spectral function is normalized according to $\int A(\omega)d\omega = 1$. As discussed in the main text, we have found unique features related to the exponential StOC in localized systems. In Fig. 9, we also plot the spectral functions for the noninteracting Anderson and interacting AA models. Distinctive features of double peaks and exponentially decaying tails are also obtained in these cases.